Electronic Supplementary Material (ESI) for Catalysis Science & Technology.

Catalytic Removal of Soot Particles Over Potassium Glasses – The Effect of Doping with Aliovalent Redox Metals

Piotr Legutko,*[a] Michał Dziadek,[b] Gabriela Grzybek,[a] Mateusz Marzec,[c] Emilia Jarosz,[a] Marek Michalik,[d] Marco Piumetti,[e] Katarzyna Cholewa-Kowalska,[b] Debora Fino[e] and Andrzej Adamski[a]

[a]*Jagiellonian University, Faculty of Chemistry, Gronostajowa 2, 30-687 Kraków, Poland*

[b]*AGH University of Science and Technology, Faculty of Materials Science and Ceramics, Mickiewicza Ave. 30, 30-059 Kraków, Poland*

[c]*AGH University of Science and Technology, Academic Centre for Materials and Nanotechnology, Mickiewicza Ave. 30, 30-059 Kraków, Poland*

[d]*Jagiellonian University, Institute of Geological Sciences, Gronostajowa 3a, 30-387 Kraków, Poland*

[e]*Politecnico do Torino, Department of Applied Science and Technology, Corso Duca degli Abruzzi 24, 10129 Torino, Italy*

*e-mail: piotr.legutko@uj.edu.pl

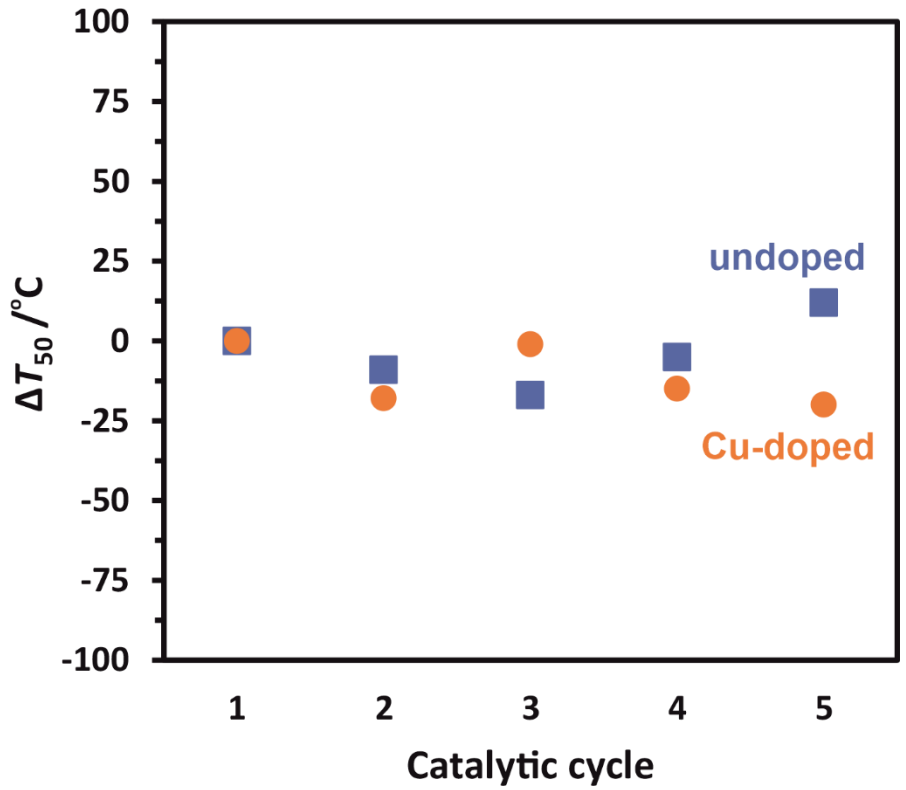

Fig. S1 Catalytic stability tests on undoped and Cu-doped glasses (*loose contact*).

Table S1 Position of the bands visible in FTIR spectra and their assignments.

Wavenumber /cm^{-1}	Band assignment	Literature
445-455	δ(O–Si–O)	1
627	δ(Si–O rings)	2
664-667	δ(O_1CO_2) in HCO_3^-	3
702-706	δ(C=O) + ν(O···H) in HCO_3^- δ(O–C–O) in CO_3^{2-}	3 4
756-770	ν_s(Si–O–Si)	1
833	π(CO_3) in HCO_3^-	3
870	π(O–C–O) in CO_3^{2-}	4,5
965	ν(Si–O^-/Si–OH)	1
1006	ν(C–O) + ν(C···O) in HCO_3^-	3
1070-1100	ν_{as}(Si–O–Si)	1
1380	ν(C–O) + ν(C···O) + δ(OHO) in HCO_3^-	3
1400	δ(OHO) in HCO_3^-	3
1430	$\nu_{as}(CO_3^{2-})$	4,5
1461	$\nu_{as}(CO_3^{2-})$	4,5
1503	$\nu_{as}(CO_3^{2-})$	4,5
1630-1680	ν(C=O)	3

ν – stretching (s – symmetric, as – asymmetric); δ - in-plane bending; π - out-of-plane bending

Table S2 Positions of the Raman bands and their assignments.

Raman shift /cm^{-1}	Band assignment	Literature
297-379	δ(Si–O–Si) in SiO_2 (Q^4)	[6,7]
466-551	δ(Si–O–Si) in SiO_2 (Q^4)	[6,7]
463	F_{2g} in CeO_2	[8]
551-621	δ(Si–O–Si) in $Si_2O_5^{2-}$ (Q^3)	[6]
595-700	δ(Si–O–Si) in $Si_2O_6^{4-}$ (Q^2)	[6,7]
847-906	ν(Si–O) in $Si_2O_6^{4-}$ (Q^2)	[6,7,9]
888-971	ν(Si–O) in $Si_2O_6^{4-}$ (Q^2)	[6,7,9]
991-1052	ν(Si–O) in $Si_2O_6^{4-}$ (Q^2)	[6,7,9]
1057-1085	ν(Si–O) in $Si_2O_5^{2-}$ (Q^3)	[6,7,9]
1120	$\nu_s(CO_3^{2-})$	[10]
1170	2LO in CeO_2	[8]

ν – stretching (s – symmetric, as – asymmetric); δ - in-plane bending

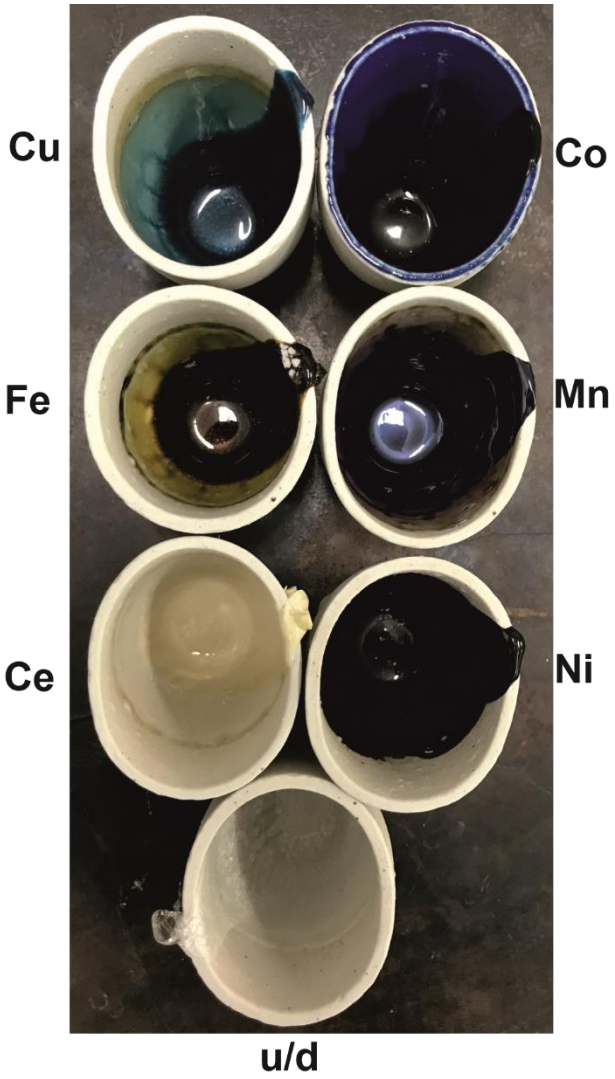

Fig. S2 The photograph of the synthesized glassy materials.

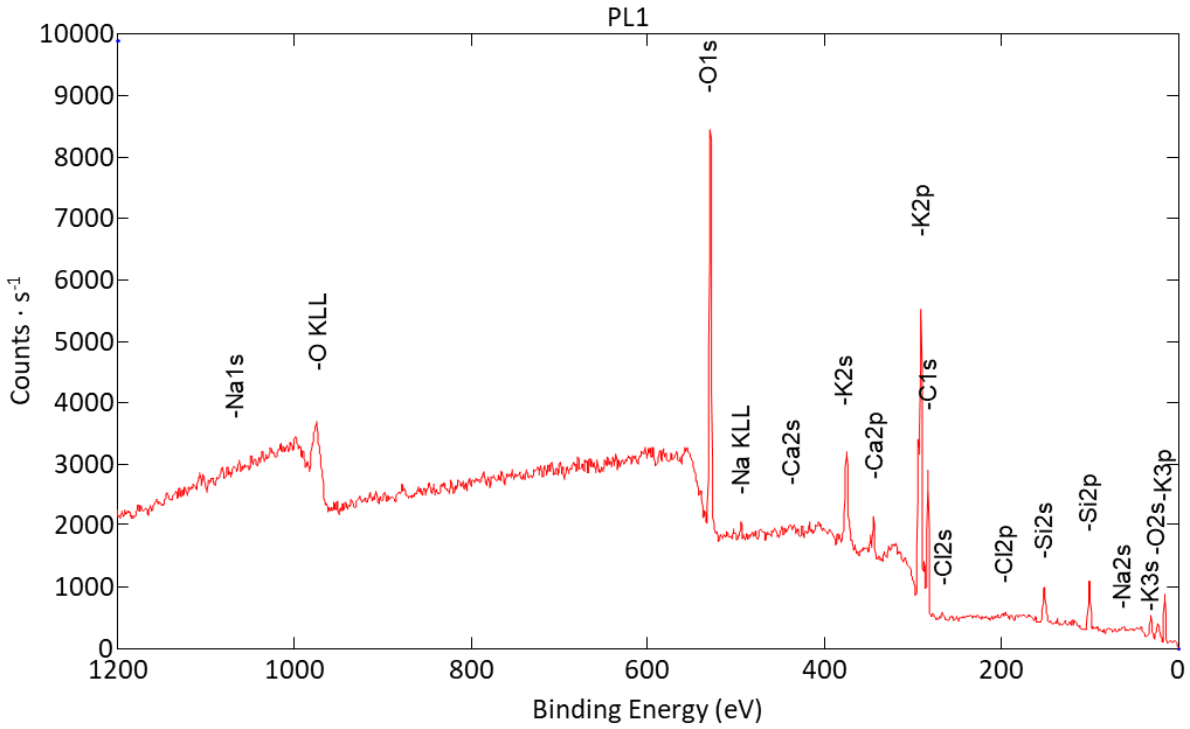

Fig. S3 XPS survey spectrum of the undoped glass.

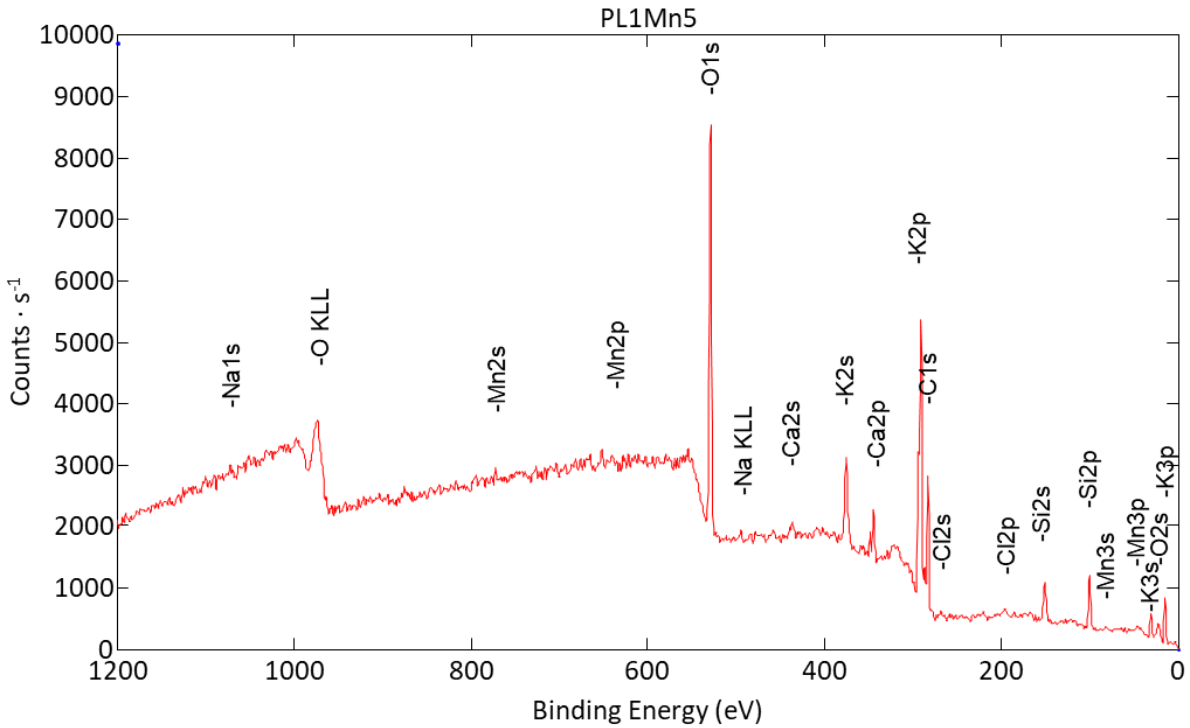

Fig. S4 XPS survey spectrum of the Mn-doped glass.

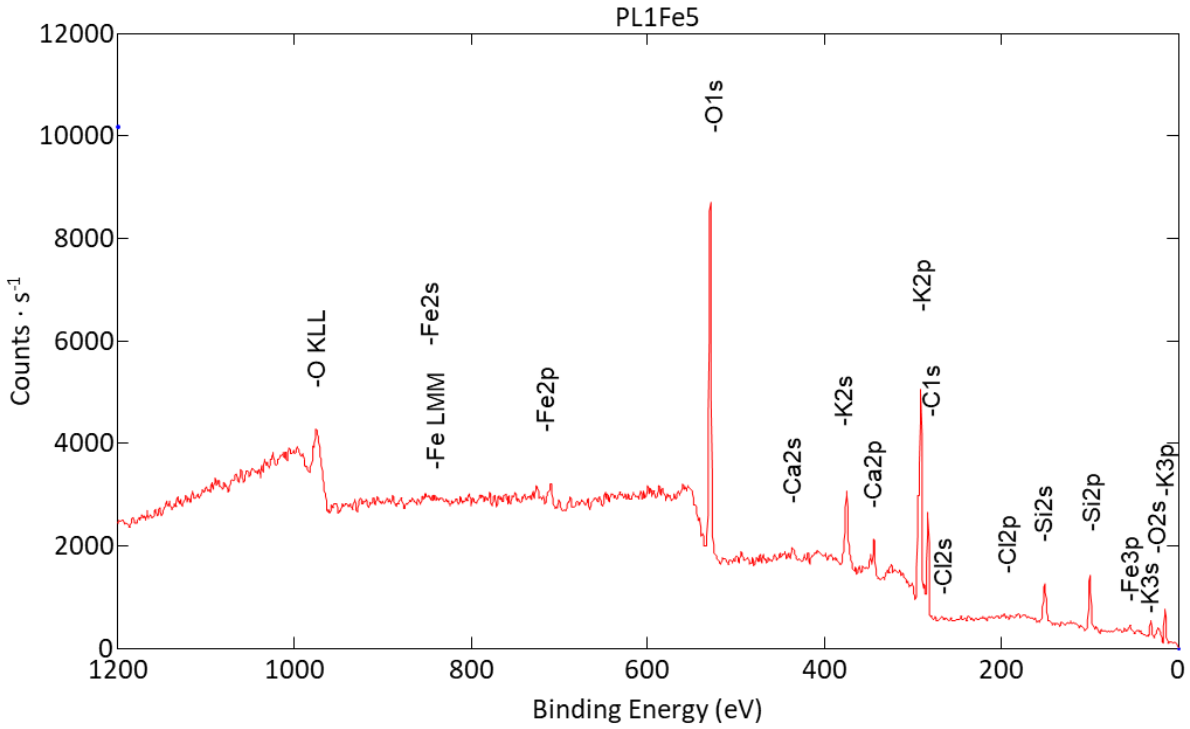

Fig. S5 XPS survey spectrum of the Fe-doped glass.

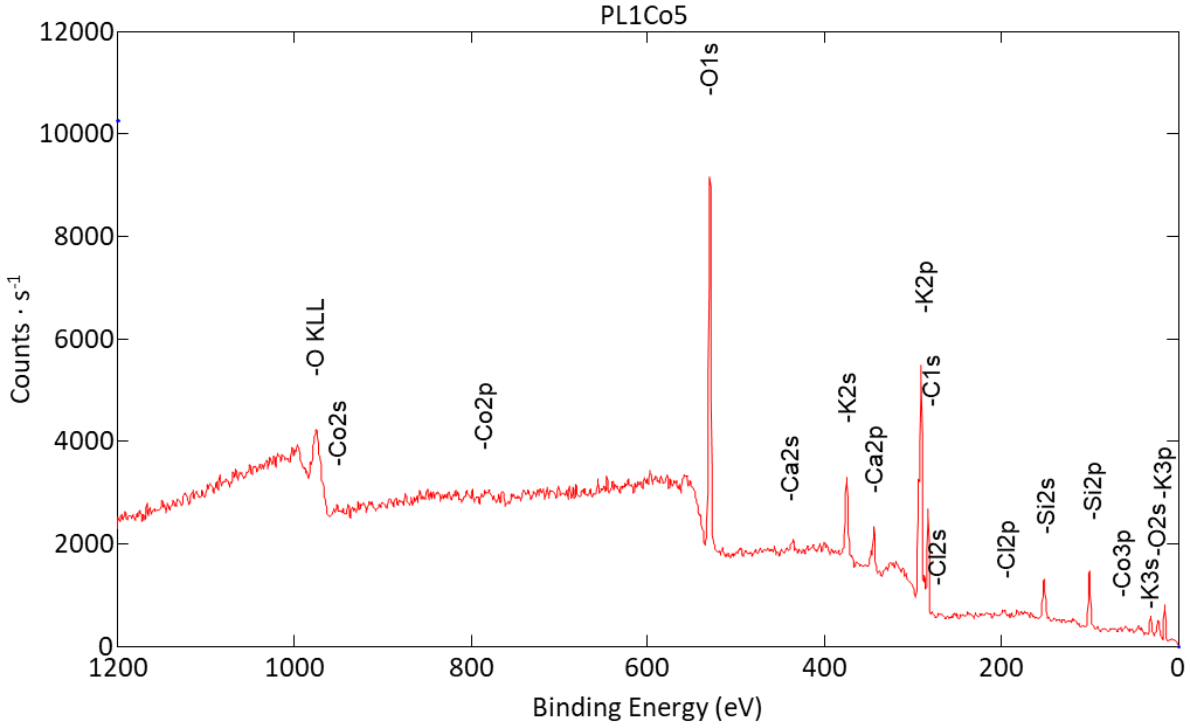

Fig. S6 XPS survey spectrum of the Co-doped glass.

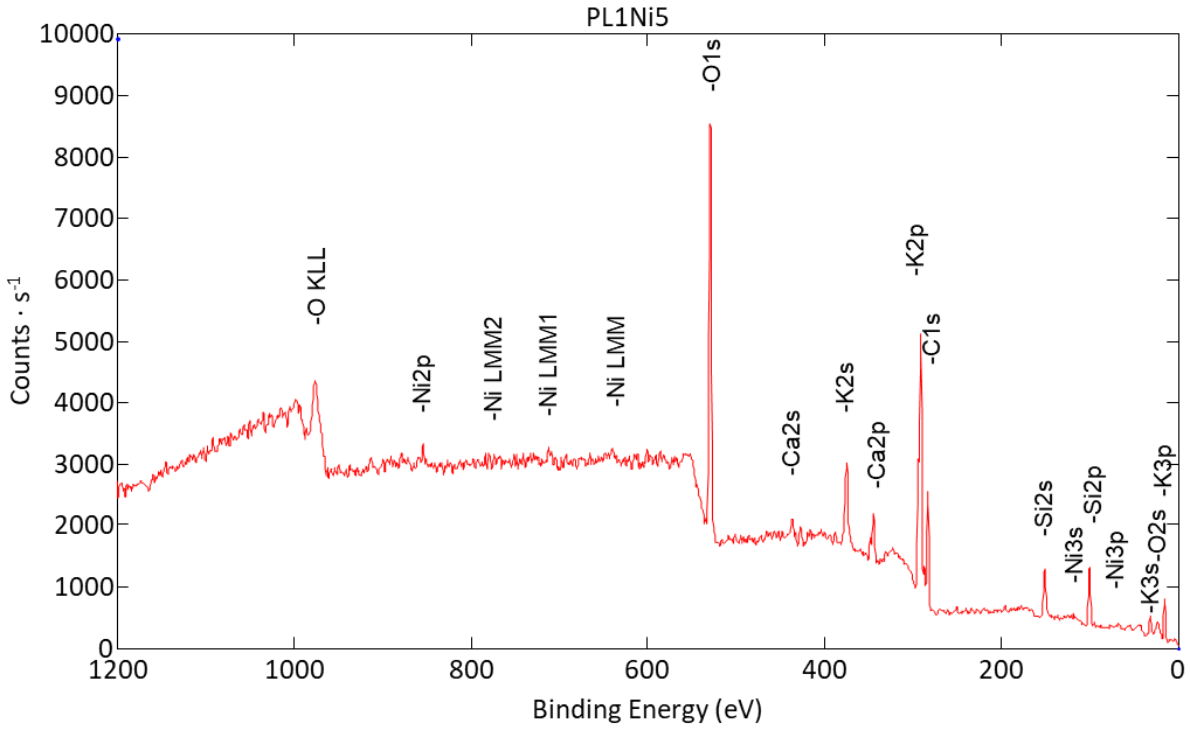

Fig. S7 XPS survey spectrum of the Ni-doped glass.

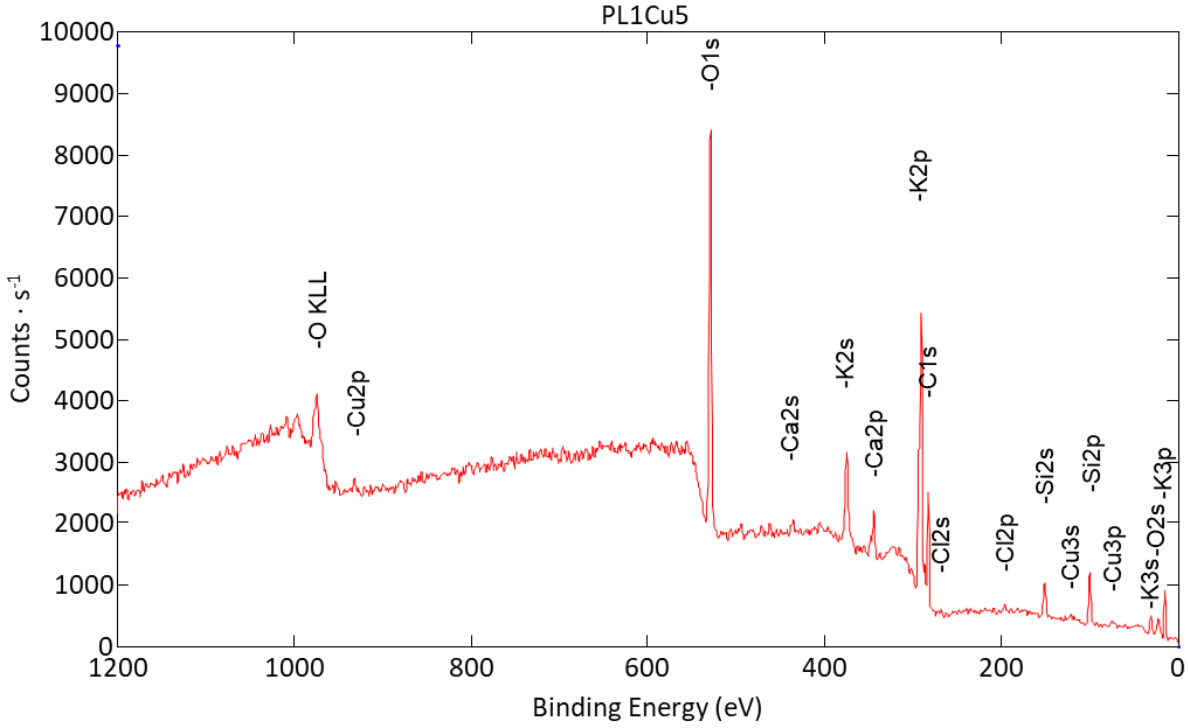

Fig. S8 XPS survey spectrum of the Cu-doped glass.

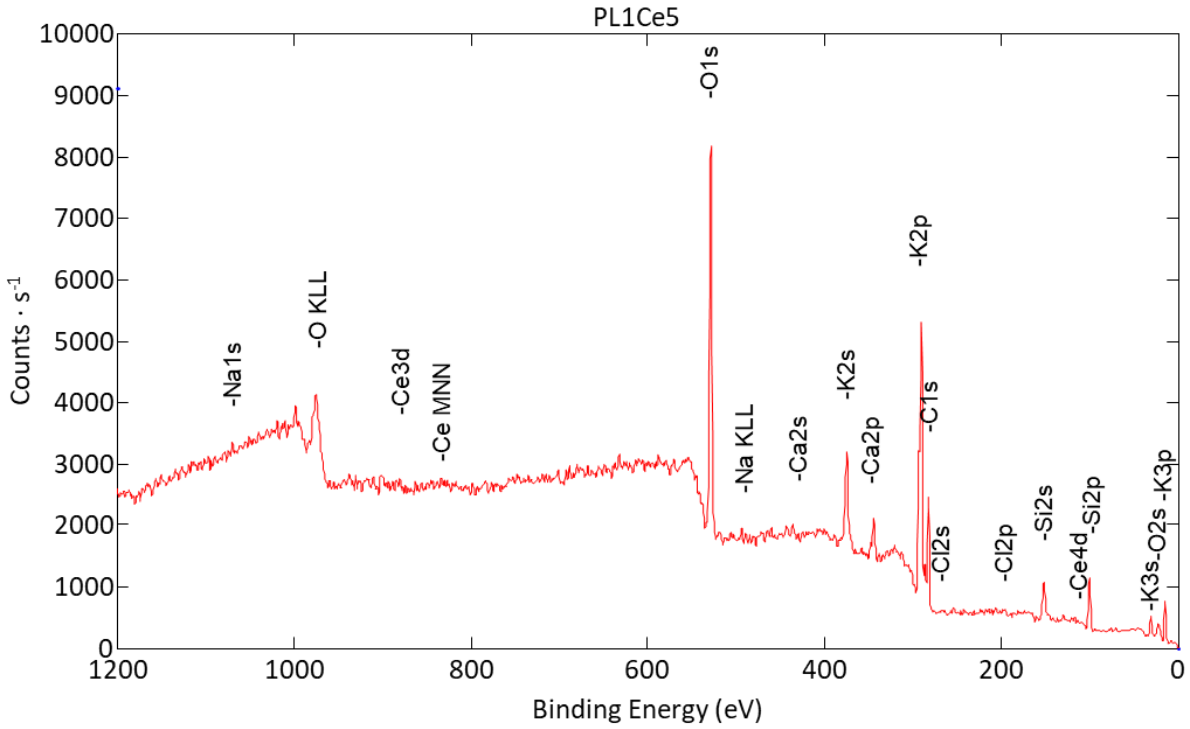

Fig. S9 XPS survey spectrum of the Ce-doped glass.

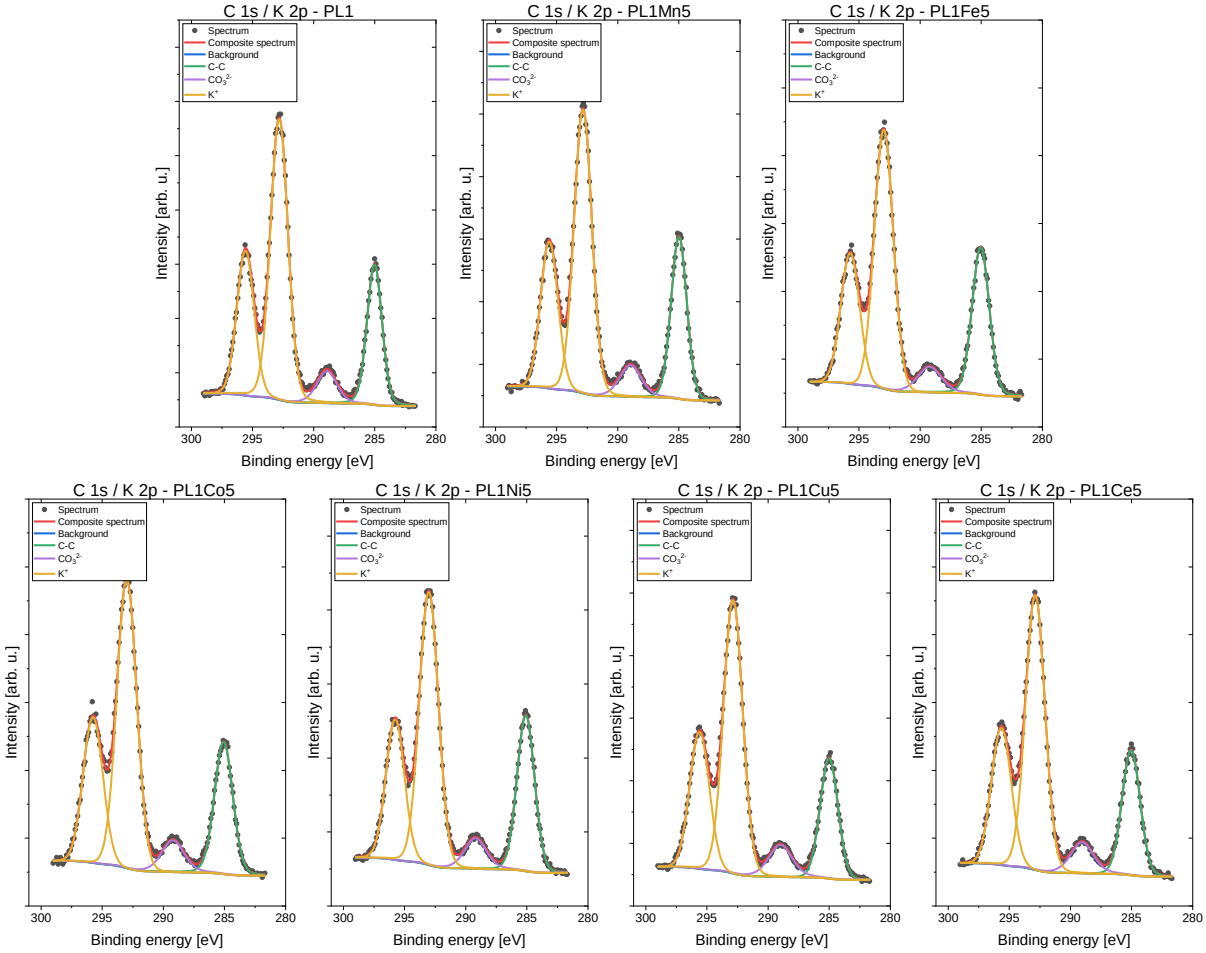

Fig. S10 HR XPS scans of C 1s and K 2p region for the investigated samples.

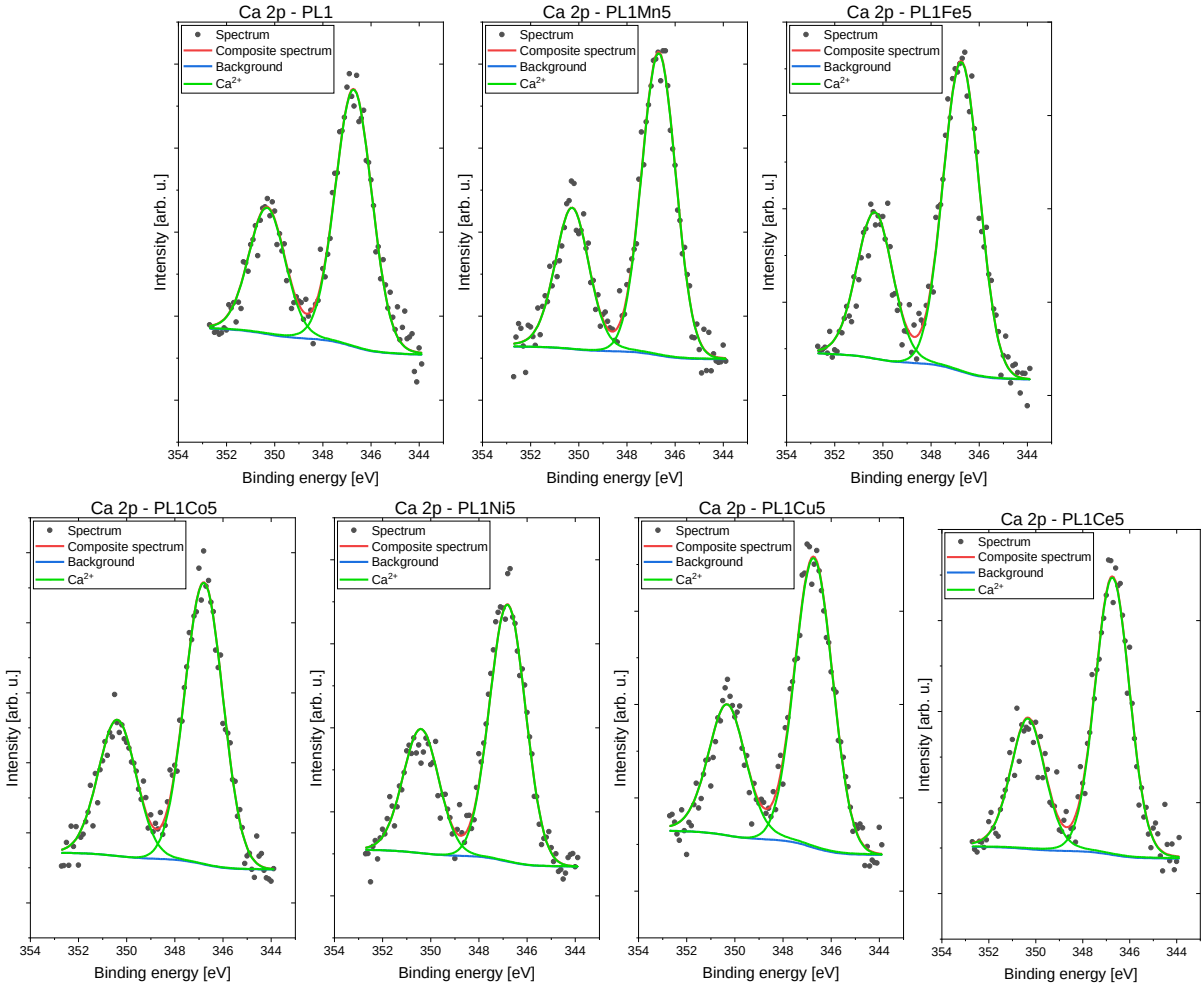

Fig. S11 HR XPS scans of Ca 2p region for the investigated samples.

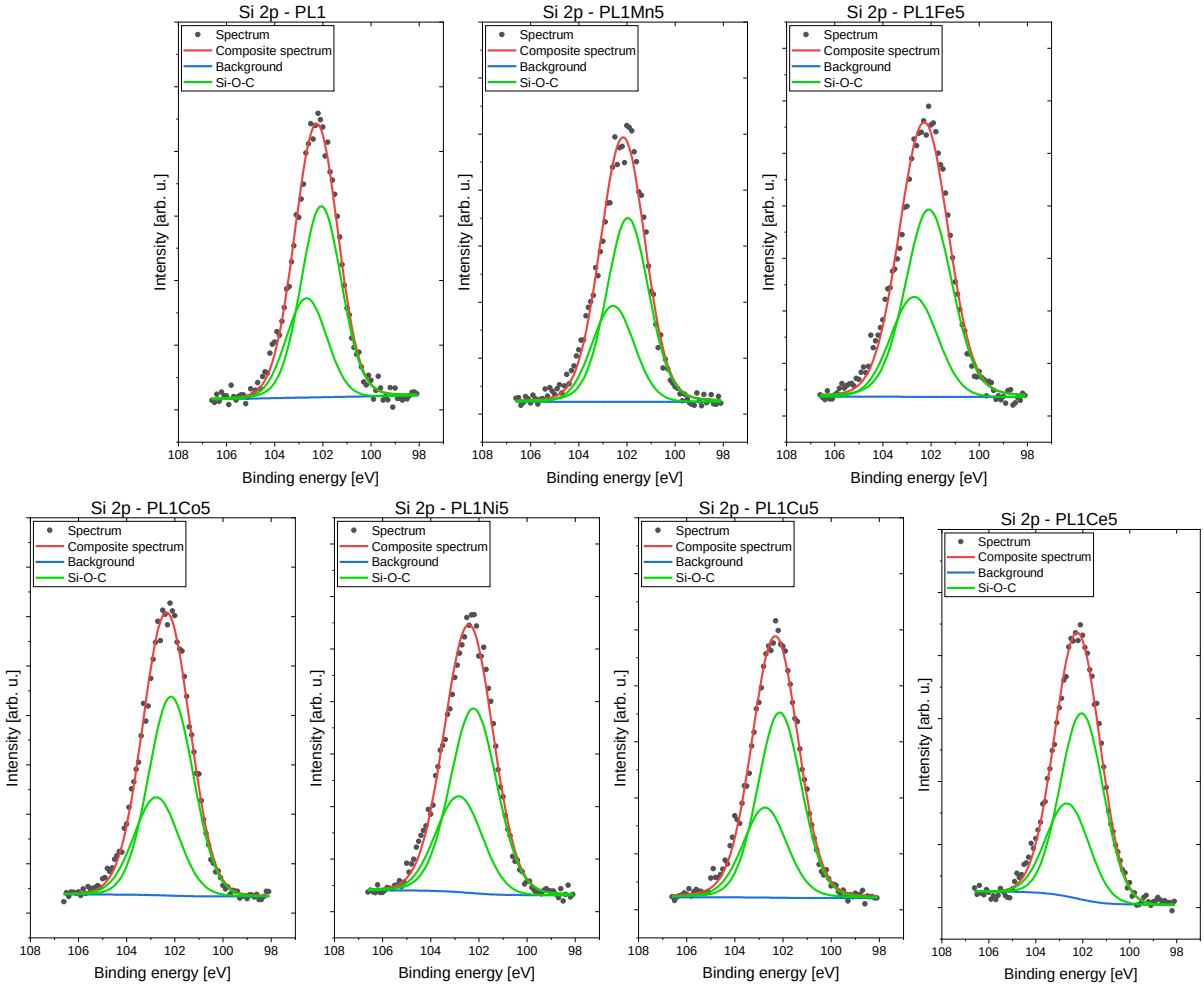

Fig. S12 HR XPS scans of Si 2p region for the investigated samples.

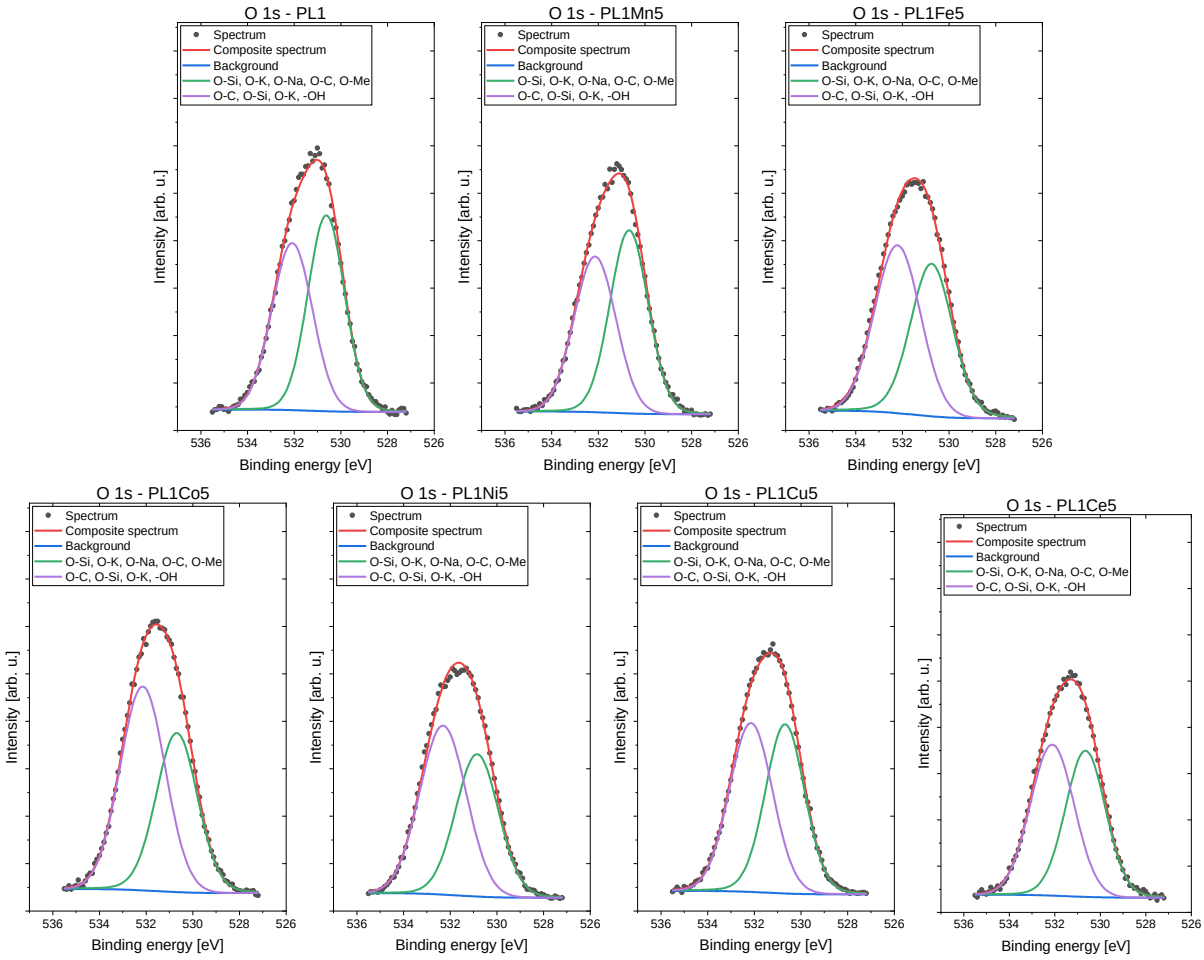

Fig. S13 HR XPS scans of O 1s region for the investigated samples.

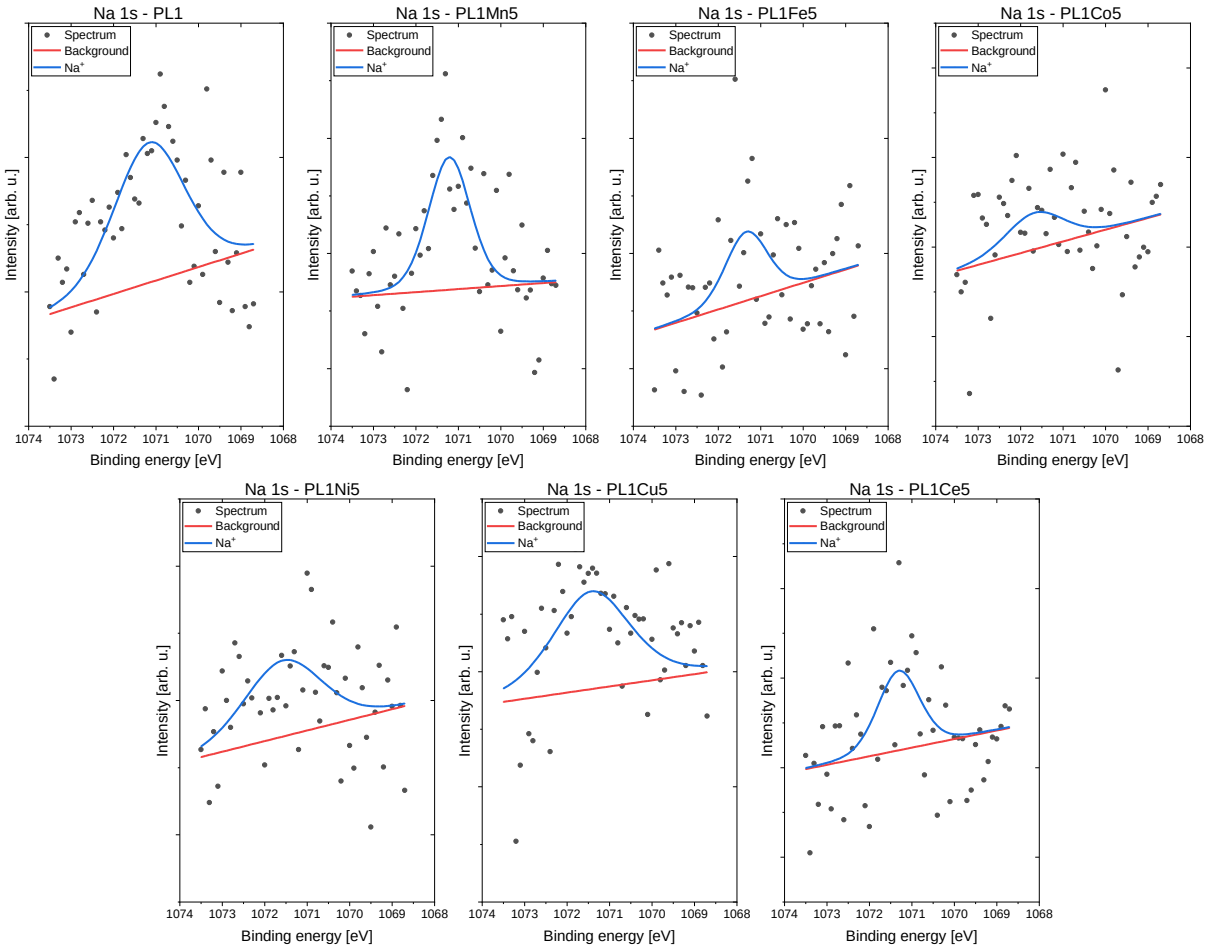

Fig. S14 HR XPS scans of Na 1s region for the investigated samples.

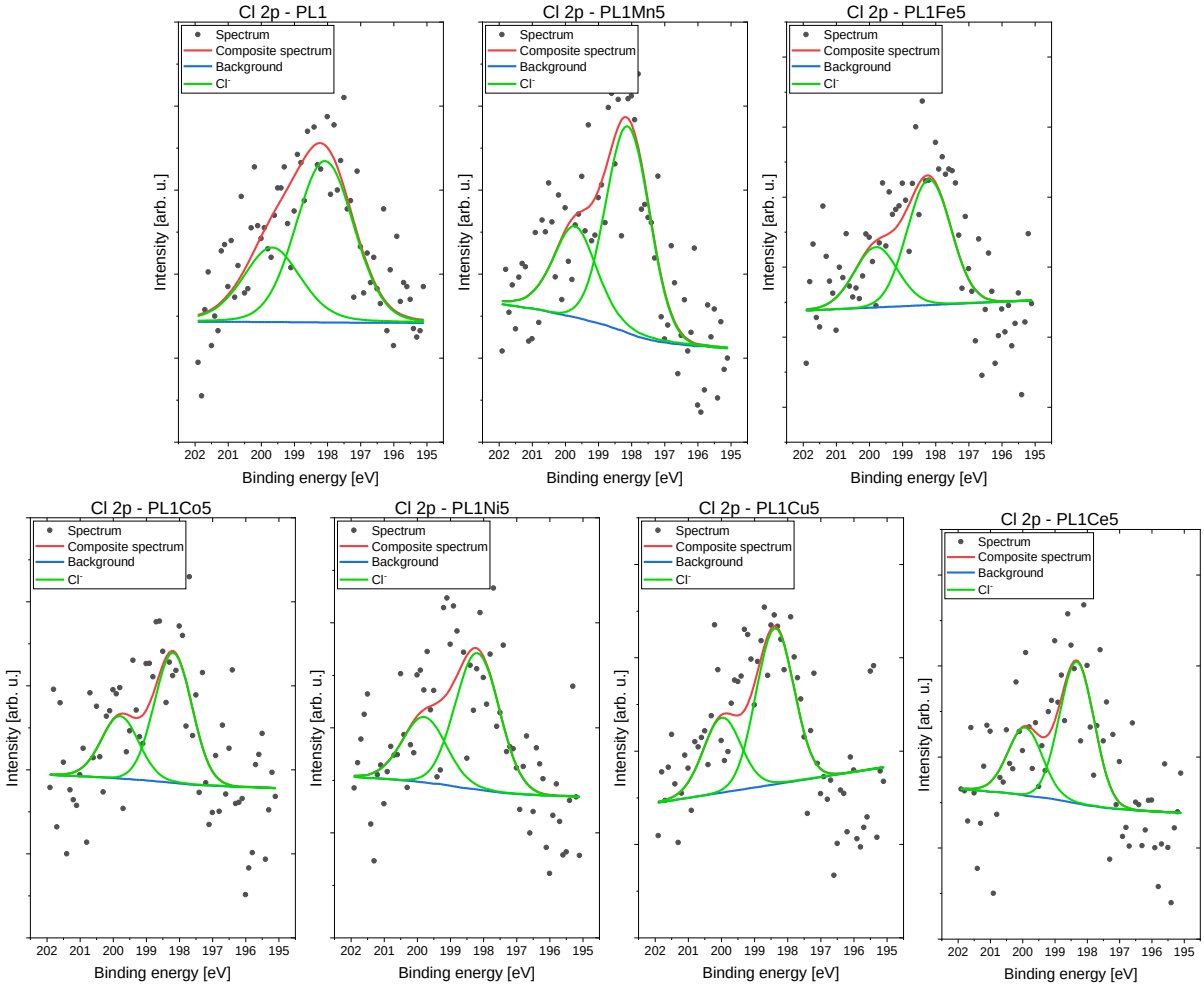

Fig. S15 HR XPS scans of Cl 2p region for the investigated samples.

Unfortunately, the determined surface concentration of dopants (Mn, Fe, Co, Ni, Cu, Ce) in the investigated samples seemed to be on the detection limit of the XPS method (Fig. S16), hence the estimation of the chemical states of the additives was rather difficult and may be burdened with an error. Anyway, the spectra collected at Mn $2p_{3/2}$ region were fitted with five components with the first line centered at 640.8 eV, which suggested the coexistence of either Mn^{2+} or Mn^{3+}. The three lines positioned within the energy range of 640 – 645 eV were due to the multiplet splitting and the position of the last shake-up line was found at ~645 eV. This line can be used as an additional parameter that confirms the $Mn^{2/3+}$ oxidation state of manganese in the samples.[11,12] Taking into account the results by UV/Vis-DR it can be stated that manganese shows a variety of oxidation states from +2 to +4 with 3+ as the predominant forms stabilized in the investigated Mn-doped glass. Fe $2p_{3/2}$ region of the XPS spectrum was fitted with four components. The first line was centered at 709.3 eV which suggested the existence of Fe^{3+} oxidation state. The three lines within the energy range of 711 – 716 eV were observed due to the multiplet splitting.[11,12] The predominant form of iron 3+ was consistent with other results reported above. The spectrum collected in the characteristic Co $2p_{3/2}$ region was fitted with four components. The first line was centered at 781.5 eV. That may indicate divalent cobalt, similar to that in CoO and/or $Co(OH)_2$.[11] The three additional lines within the energy

range of 784-790 eV were also due to the corresponding multiplet splitting. The Ni $2p_{3/2}$ spectrum was fitted with three lines. The first line was positioned at 855.9 eV, indicating the Ni^{2+} oxidation state, like in the case of nickel oxide NiO and/or hydroxide.[11,13,14] The Cu $2p_{3/2}$ spectrum was fitted with a single line centered at 933.2 eV which indicated, together with a lack of satellite features in the range of 940 – 945 eV, the presence of Cu in either metallic or +1 oxidation state, like in Cu_2O.[15–17] UV/Vis-DR results confirmed that Cu^{2+} was also present in the synthesized sample, which might be slightly inconsistent with XPS. However, the population of Cu^{2+} centers exposed to the surface might be very small. The Ce 3d spectrum was fitted with four doublet structures ($d_{5/2}$ – $d_{3/2}$ doublet separation equals 18.6 eV) that can arise from two chemical states of Ce but due to the multiplet splitting phenomena, each chemical state was further split. Eight lines were applied to accurately fit the spectra (four doublets – two from Ce(III) and two from Ce(IV)). Those four doublets applied for fitting suggested the coexistence of both Ce(III) and Ce(IV) states.[18,19] These results are consistent with other data reported for the studied samples.

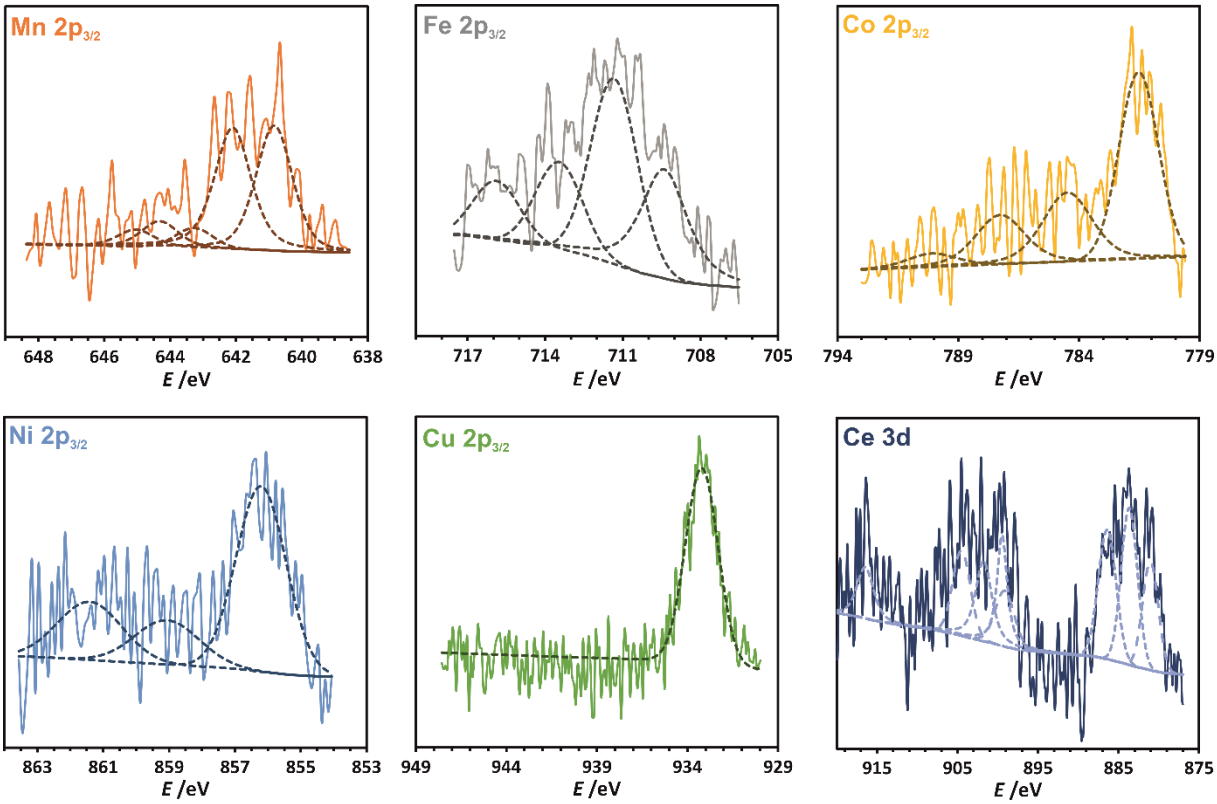

Fig. S16 XPS regions characteristic of the dopants introduced into the investigated glasses.

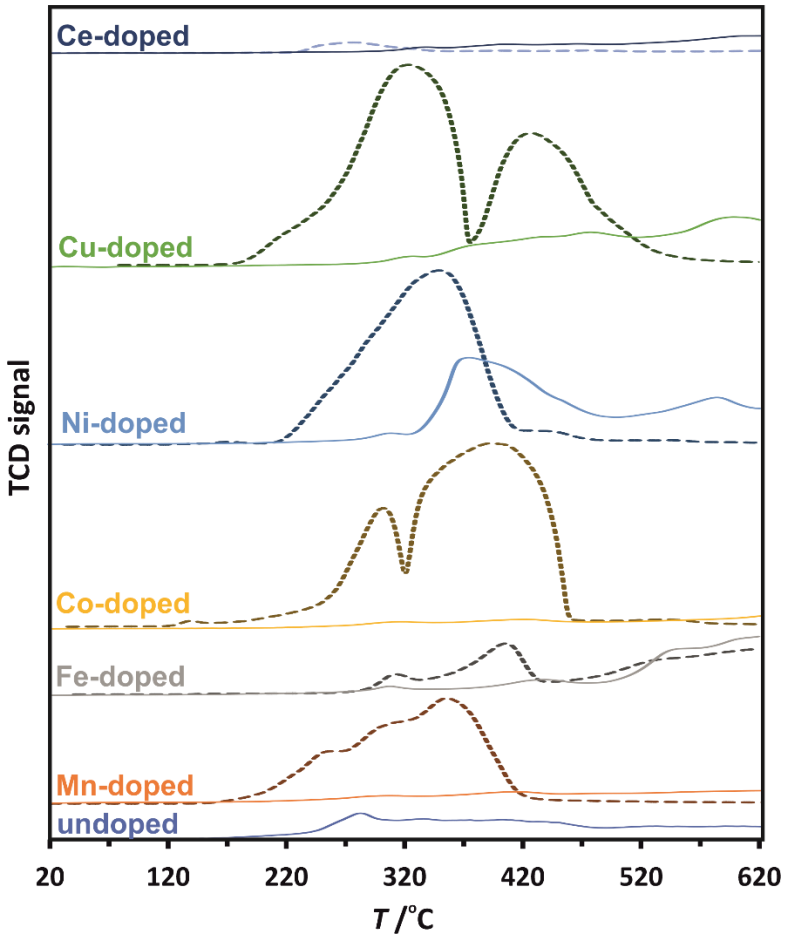

Fig. S17 H_2-TPR profiles of the investigated potassium glasses together with profiles of corresponding doping oxides (dotted lines).

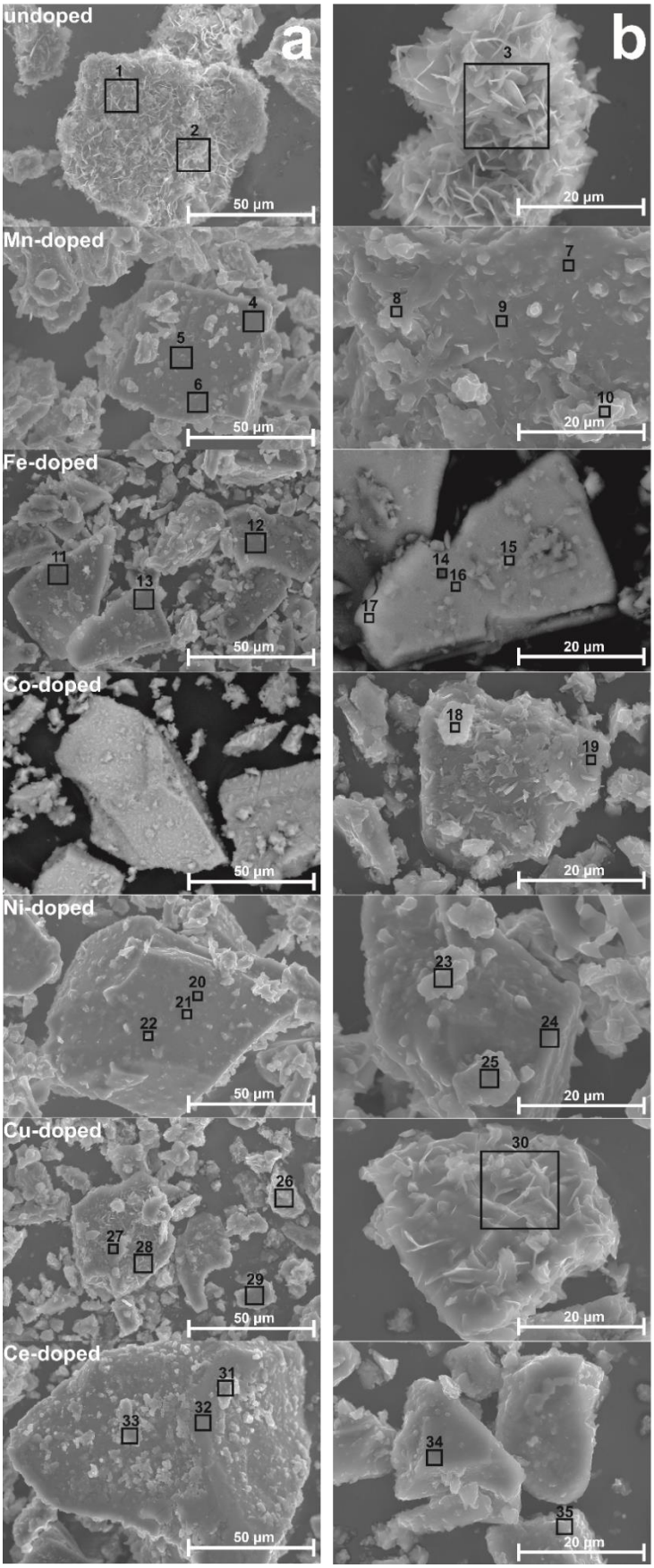

Fig. S18 SEM images of the investigated glasses: magnification 1000 (a) and 2500 (b) times. Areas analyzed by EDX were marked by squares and numbered.

Table S3 The composition of the undoped glass determined by EDX – regions indicated in Fig. S17.

	Region 1	**Region 2**	**Region 3**
Si /at. %	26.14	20.65	23.26
K /at. %	23.31	34.71	33.68
Ca /at. %	8.54	11.28	10.98
O /at. %	40.73	31.85	30.39

Table S4 The composition of the Mn-doped glass determined by EDX – regions indicated in Fig. S17.

	Region 4	**Region 5**	**Region 6**	**Region 7**	**Region 8**	**Region 9**	**Region 10**
Si /at. %	24.77	25.04	29.32	24.18	23.45	10.49	27.30
K /at. %	19.80	21.13	32.38	44.67	43.19	53.89	19.65
Ca /at. %	6.61	7.68	10.91	15.10	6.95	11.01	8.36
O /at. %	45.16	42.66	22.61	8.21	20.84	13.41	40.22
Mn /at. %	2.05	2.26	3.73	7.85	4.57	11.20	2.66

Table S5 The composition of Fe-doped glass determined by EDX – regions indicated in Fig. S17.

	Region 11	**Region 12**	**Region 13**	**Region 14**	**Region 15**	**Region 16**	**Region 17**
Si /at. %	25.07	25.22	25.63	28.51	24.77	27.41	23.49
K /at. %	21.40	21.01	20.91	22.51	15.18	23.38	16.84
Ca /at. %	7.89	7.79	7.85	6.90	7.16	9.18	6.79
O /at. %	39.90	40.15	39.49	35.03	47.62	32.99	47.41
Fe /at. %	4.71	4.66	4.90	6.45	4.40	6.11	4.42

Table S6 The composition of Co-doped glass determined by EDX – regions indicated in Fig. S17.

	Region 18	**Region 19**
Si /at. %	23.50	25.97
K /at. %	13.09	19.43
Ca /at. %	4.97	7.92
O /at. %	55.21	42.14
Co /at. %	1.78	2.47

Table S7 The composition of Ni-doped glass determined by EDX – regions indicated in Fig. S17.

	Region 20	Region 21	Region 22	Region 23	Region 24	Region 25
Si /at. %	29.98	25.70	24.32	19.75	23.95	27.40
K /at. %	26.98	29.65	11.86	18.95	20.69	26.17
Ca /at. %	10.15	8.84	6.01	7.35	7.53	7.55
O /at. %	26.06	30.61	53.27	50.31	43.37	33.02
Ni /at. %	6.10	4.37	3.26	2.74	3.35	5.23

Table S8 The composition of Cu-doped glass determined by EDX – regions indicated in Fig. S17.

	Region 26	Region 27	Region 28	Region 29	Region 30
Si /at. %	18.75	26.03	25.98	23.32	20.37
K /at. %	21.07	18.05	28.83	20.35	15.12
Ca /at. %	9.14	7.06	10.41	7.80	5.81
O /at. %	47.86	45.97	30.45	44.64	55.65
Cu /at. %	1.71	1.93	3.34	2.35	1.47

Table S9 The composition of Ce-doped glass determined by EDX – regions indicated in Fig. S17.

	Region 31	Region 32	Region 33	Region 34	Region 35
Si /at. %	22.70	25.34	20.62	26.21	23.35
K /at. %	17.95	21.87	23.09	21.22	13.64
Ca /at. %	6.02	7.10	5.80	7.62	5.61
O /at. %	51.33	43.62	48.17	42.74	55.07
Ce /at. %	1.06	1.19	1.17	1.18	1.11

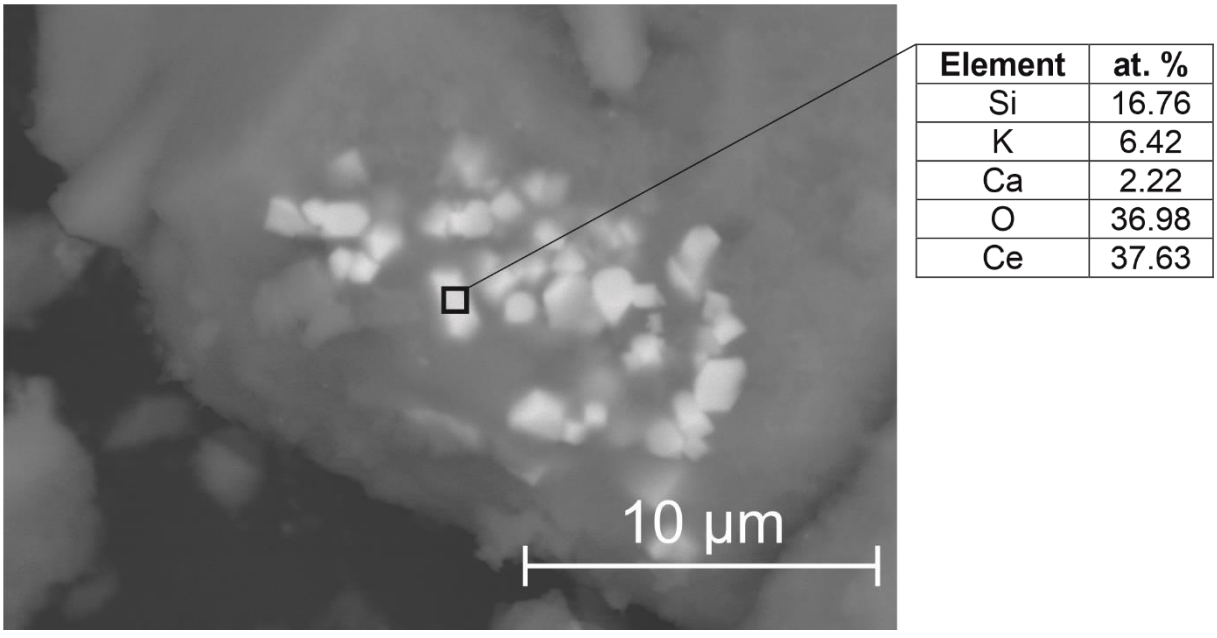

Fig. S19 SEM image of Ce-doped glass with visible CeO_2 domains.

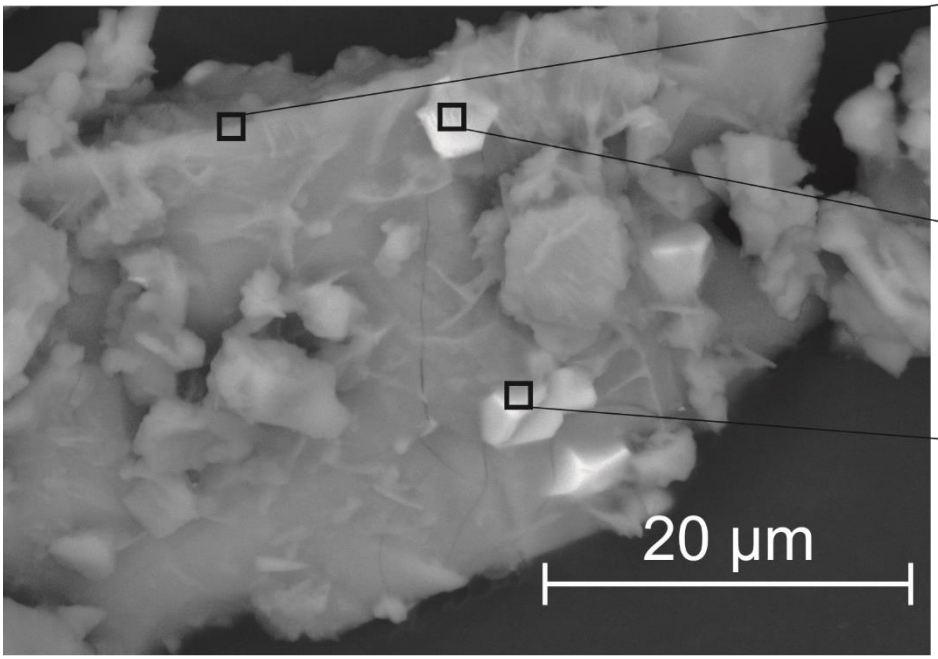

Element	at. %
Si	32.28
K	26.71
Ca	10.80
O	25.69
Ni	3.94

Element	at. %
Si	8.52
K	7.00
Ca	2.20
O	6.46
Ni	75.8

Element	at. %
Si	8.79
K	4.50
Ca	0.98
O	5.61
Ni	80.1

Fig. S20 SEM image of Ni-doped glass with visible NiO domains.

References

1 H. Liu, H. Kaya, Y. T. Lin, A. Ogrinc and S. H. Kim, *J. Am. Ceram. Soc.*, 2022, **105**, 2355–2384.

2 M. Sitarz, M. Handke and W. Mozgawa, *Spectrochim. Acta - Part A Mol. Biomol. Spectrosc.*, 2000, **56**, 1819–1823.

3 K. Nakamoto, Y. Anantaeama Saema and H. Ogoshi, *J. Chem. Phys.*, 1965, **43**, 1177–1181.

4 M. H. Brooker and J. B. Bates, *Spectrochim. Acta Part A Mol. Spectrosc.*, 1974, **30**, 2211–2220.

5 S. M. Barinov, J. V. Rau, S. N. Cesaro, J. Ďurišin, I. V. Fadeeva, D. Ferro, L. Medvecky and G. Trionfetti, *J. Mater. Sci. Mater. Med.*, 2006, **17**, 597–604.

6 L. Robinet, C. Coupry, K. Eremin and C. Hall, *J. Raman Spectrosc.*, 2006, **37**, 789–797.

7 T. Seuthe, M. Grehn, A. Mermillod-Blondin, H. J. Eichler, J. Bonse and M. Eberstein, *Opt. Mater. Express*, 2013, **3**, 755.

8 C. Schilling, A. Hofmann, C. Hess and M. V. Ganduglia-Pirovano, *J. Phys. Chem. C*, 2017, **121**, 20834–20849.

9 M. T. Nayak and J. A. E. Desa, *J. Raman Spectrosc.*, 2018, **49**, 1507–1513.

10 Y. Morizet, R. A. Brooker, G. Iacono-Marziano and B. A. Kjarsgaard, *Am. Mineral.*, 2013, **98**, 1788–1802.

11 M. C. Biesinger, L. W. M. Lau, A. R. Gerson and R. S. C. Smart, *Appl. Surf. Sci.*, 2010,

257, 887–898.

12 A. P. Grosvenor, B. A. Kobe, M. C. Biesinger and N. S. McIntyre, *Surf. Interface Anal.*, 2004, **36**, 1564–1574.

13 M. C. Biesinger, L. W. M. Lau, A. R. Gerson and R. S. C. Smart, *Phys. Chem. Chem. Phys.*, 2012, **14**, 2434–2442.

14 M. C. Biesinger, B. P. Payne, L. W. M. Lau, A. Gerson and R. S. C. Smart, *Surf. Interface Anal.*, 2009, **41**, 324–332.

15 M. C. Biesinger, *Surf. Interface Anal.*, 2017, **49**, 1325–1334.

16 P. C. Healy, S. Myhra and A. M. Stewart, *Jpn. J. Appl. Phys.*, 1987, **26**, L1884–L1887.

17 N. S. Mcintyre and M. G. Cook, *Anal. Chem.*, 1975, **47**, 2208–2213.

18 A. E. Nelson and K. H. Schulz, *Appl. Surf. Sci.*, 2003, **210**, 206–221.

19 D. R. Mullins, S. H. Overbury and D. R. Huntley, *Surf. Sci.*, 1998, **409**, 307–319.